



PERGAMON

Journal of the Mechanics and Physics of Solids  
49 (2001) 635–654

---

---

JOURNAL OF THE  
MECHANICS AND  
PHYSICS OF SOLIDS

---

---

www.elsevier.com/locate/jmps

# The effect of crack blunting on the competition between dislocation nucleation and cleavage

Lisa L. Fischer, Glenn E. Beltz \*

*Department of Mechanical and Environmental Engineering, University of California, Santa Barbara, CA 93106-5070, USA*

Received 14 October 1999; received in revised form 20 June 2000

---

## Abstract

To better understand the ductile versus brittle fracture behavior of crystalline materials, attention should be directed towards physically realistic crack geometries. Currently, continuum models of ductile versus brittle behavior are typically based on the analysis of a pre-existing sharp crack in order to use analytical solutions for the stress fields around the crack tip. This paper examines the effects of crack blunting on the competition between dislocation nucleation and atomic decohesion using continuum methods. We accomplish this by assuming that the crack geometry is elliptical, which has the primary advantage that the stress fields are available in closed form. These stress field solutions are then used to calculate the thresholds for dislocation nucleation and atomic decohesion. A Peierls-type framework is used to obtain the thresholds for dislocation nucleation, in which the region of the slip plane ahead of the crack develops a distribution of slip discontinuity prior to nucleation. This slip distribution increases as the applied load is increased until an instability is reached and the governing integral equation can no longer be solved. These calculations are carried out for various crack tip geometries to ascertain the effects of crack tip blunting. The thresholds for atomic decohesion are calculated using a cohesive zone model, in which the region of the crack front develops a distribution of opening displacement prior to atomic decohesion. Again, loading of the elliptical crack tip eventually results in an instability, which marks the onset of crack advance. These calculations are carried out for various crack tip geometries. The results of these separate calculations are presented as the critical energy release rates versus the crack tip radius of curvature for a given crack length. The two threshold curves are compared simultaneously to determine which failure mode is energetically more likely at various crack tip curvatures. From these comparisons, four possible types of material fracture behavior are identified: intrinsically brittle, quasi-brittle, intrinsically ductile, and quasi-ductile. Finally, real material examples are discussed. © 2001 Elsevier Science Ltd. All rights reserved.

*Keywords:* Crack blunting; Dislocation nucleation; Cleavage; Atomic decohesion; Ductile vs. brittle behavior

---

\* Corresponding author. Tel.: +1-805-893-3354; fax: +1-805-893-8651.  
E-mail address: beltz@engineering.ucsb.edu (G.E. Beltz).

## 1. Introduction

For some time, theoretical analyses of the competition between ductile and brittle material behavior have specifically addressed the competition between dislocation nucleation at a crack tip and cleavage. Rice and Thomson (1974) were among the first to consider this problem by specifically making use of elasticity solutions to solve for the thresholds to emit a fully formed dislocation on a slip plane intersecting the crack tip. The load for dislocation nucleation was then compared with the load required for Griffith cleavage. Later versions of the Rice–Thomson model characterized this competition in terms of critical energy release rates  $G_{\text{cleave}}$  for cleavage, and  $G_{\text{disl}}$  for dislocation emission. In these studies, the event possessing the lowest critical energy release rate was predicted to dominate. Emission of a single dislocation was thought to imply that the material would continue to emit dislocations, thus “shielding” the stress singularity and preventing further brittle fracture. If cleavage was predicted, brittle fracture would persist.

Rice (1992) made a great step in advancing the sophistication of these types of analyses when he introduced a model that incorporated the Peierls (1940) dislocation description. Assuming a periodic relationship between the shear stress and slip displacement along the slip plane intersecting the crack tip, this model solves for a distribution of slip displacement that results from far field loading using a nonlinear integral equation. Eventually, after increasing the applied load and evaluating the resulting slip displacement distribution, an instability is reached, and the integral equation no longer has a stable solution. This instability marks the nucleation of a dislocation from the crack tip. The advantage of this approach is that it avoids any use of a core cutoff approximation for the dislocation, while providing a physically realistic mechanism for the formation of an incipient dislocation core prior to nucleation.

Over the years, this framework has been broadened by Rice et al. (1992) and Xu et al. (1995, 1997) to account for elastic anisotropy, cracks on bimaterial interfaces, extended core structures, realistic slip systems, and three-dimensional dislocation geometries. Despite many improvements made in later versions of the Rice–Thomson model, one assumption has typically been made: crack tips are initially atomically sharp, and remain so during and subsequent to dislocation nucleation. In the current work, we adopt the viewpoint that a “pre-blunted” crack may be used as a reference configuration from which a study of dislocation nucleation versus cleavage may be undertaken. We envision a crack that is continuously blunting on the atomic scale due to (but not limited to) previous crack tip dislocation nucleation, anelastic deformation, diffusion of atoms from the crack tip region, or chemical reactions. The analysis would also apply if a blunt notch were introduced artificially, through cutting or some other mechanical process.

Atomic models for cracks have yielded important results pertaining to crack blunting, and the drive to reconcile continuum models with atomistic simulation results provides a further impetus for our current study. For example, Gumbsch (1995) and Gumbsch and Beltz (1995) used a hybrid finite element-atomistic mesh (FE-At) to compare the load required for brittle fracture with various continuum-based criteria and found good agreement with simple mode I–II loadings where the slip plane coincided with the

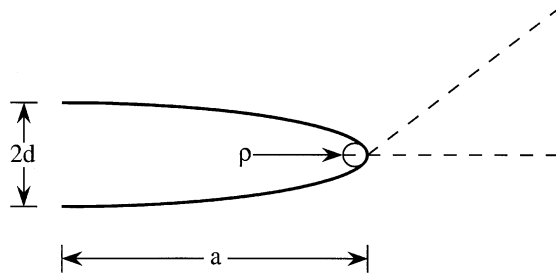


Fig. 1. A diagram of half of an elliptical crack. The ellipse has a major axis of  $2a$  and a minor axis of  $2d$ . The radius of curvature of the crack tip is given by  $\rho = d^2/a$ . The slip plane, inclined at angle  $\theta$ , intersects the crack tip.

crack plane (in these cases, dislocation nucleation does *not* result in blunting or ledge formation). In cases where dislocation nucleation does result in blunting, the FE-At and continuum results did not give perfect agreement. As an additional example, Schiøtz et al. (1996, 1997) studied the effects of blunt crack geometries on crack propagation. Static simulations were conducted using a two-dimensional hexagonal lattice under mode I and mode II loading. They found that for a “blunting height” of 10 layers of atoms, the force required to propagate the crack was 15–20% more than that for an atomically sharp crack. Other examples include molecular dynamic simulations by Dienes and Paskin (1987), Paskin et al. (1985), and Farkas (1998a,b, 1999), which overwhelmingly suggest that blunting of a sharp crack tip can significantly modify the stress field around the crack tip, and/or change the favorability of crack advance or dislocation nucleation.

In this paper, we propose to assess the fracture behavior of crystalline materials by considering the ongoing competition between dislocation nucleation and crack injection in blunted crack tip configurations via continuum methods. A blunted crack tip configuration that is analytically tractable is used to simulate crack tip blunting at the dislocation length scale. In this approach, two governing integral equations for dislocation nucleation and crack advance are developed. The solutions for the stress fields, or “kernels”, used in these equations can be found in the literature and can be manipulated into their required form in order to solve for the dislocation nucleation and atomic-decohesion thresholds. These two threshold solutions are compared for varying values of crack tip bluntness, and we demonstrate that four separate cases of material fracture behavior can result. Using this method, predictions are made about the fracture behavior of several real materials.

## 2. General description of model

In order to quantify crack blunting, we model the crack as a slender, elliptical cut-out centered in an infinite medium. The ellipse shown in Fig. 1 has a major axis of  $2a$  and a minor axis of  $2d$ . The crack tip radius of curvature, given by  $\rho = d^2/a$ , is a measure of the “bluntness” of the crack tip. Crack advance, or “injection”, is

assumed to occur directly ahead of the crack tip, and dislocation nucleation is assumed to occur on the slip plane inclined at angle  $\theta$  that intersects the elliptical crack tip. The model is completely two-dimensional (plane strain), and the dislocation lines are assumed to parallel the crack front. Dislocations that have a screw component (Burgers vector component parallel to the crack front) are not considered in this paper. An obvious trade-off here is that the elliptical crack tip profile does not retain the corner (and its associated stress singularity) that would result, at least from a continuum viewpoint, when dislocations emit along the slip plane – suggesting that our elliptical representation will lead to an overestimate of the effects of blunting. We suggest that the notion of a sharp corner is unrealistic at the atomic scale – not only because it cannot not be defined, but because local atomic motions and relaxations are always occurring. Our basic premise is to have some length scale that quantifies crack blunting on the atomic scale, in order to uncover general trends, while the exact shape to be analyzed is a secondary detail. Future work should address the issue of rounded versus sharp corners, however.

To calculate the energy release rate for dislocation nucleation (Section 3), a Peierls-type treatment similar to that proposed by Rice (1992) is applied to the active slip plane of the elliptical crack tip. The Peierls treatment assumes there is a periodic relationship between shear stress and slip displacement along the slip plane intersecting the crack tip. A nonlinear integral equation can be written, the solution to which must balance the stress due to applied loads (assuming a completely elastic solid) at some position  $r$  along the slip plane, the slip displacement stress at that position  $r$ , and the stress at position  $r$  due to slip displacement along the remainder of the slip plane. Immediately prior to dislocation nucleation, there exists a distribution of slip discontinuity along the slip plane that is unstable with respect to further increases in applied stress, and the dislocation is said to nucleate at that point. The load at which this instability occurs is then used to determine the critical energy release rate associated with nucleation.

To calculate the energy release rate for crack propagation (Section 4), a cohesive zone model is used. The cohesive zone calculations are very similar to the Peierls calculations in that a nonlinear relationship between the opening stress and the opening displacement is assumed. Again, a governing integral equation can be written to balance the stress due to applied loads, the stress due to opening displacement, and the stress due to opening displacement along the rest of the crack front for every point along the crack front. With increasing applied stress, a distribution of opening displacement develops in the region ahead of the crack tip. Ultimately, an instability is reached and the crack is said to advance. The load applied at the moment of the instability is then used to calculate the energy release rate associated with crack injection. The process (dislocation nucleation or crack advance) which results in the lowest energy release rate is then favored.

### **3. Dislocation nucleation**

First, we consider an elliptical crack (Fig. 1) subject to remote, uniaxial tension (i.e., mode I fracture). The shear stresses along the slip plane due to the applied loading are

needed for this analysis, as well as the shear “self-stresses” due to an edge dislocation situated arbitrarily along the slip plane. These shear stress solutions are found following the work of Muskhelishvili (1975) and Vitek (1975). Once the applicable stress fields have been determined, the critical loads for dislocation nucleation are calculated for various crack lengths and crack tip radii of curvature. The calculations reveal that increasing crack length or crack-tip radius of curvature generally increases the critical energy release rate for dislocation nucleation under mode I loading.

In order to solve for the shear stress along the slip plane due to the uniaxial loading, conformal mapping is used. Specifically, the ellipse in the complex  $z$ -plane is mapped to a unit circle in the  $\zeta$ -plane

$$z = \left( \frac{a+d}{2} \right) \zeta + \left( \frac{a-d}{2} \right) \frac{1}{\zeta} = R \left( \zeta + \frac{m}{\zeta} \right), \quad (1)$$

where  $z = x + iy$ ,  $R \equiv (a+d)/2$ , and  $m \equiv (a-d)/(a+d)$ .

Next, a plane with no crack or hole, subject to uniaxial loading  $\sigma$  in the vertical direction, is considered. For this case, the principal stress components are  $\sigma_{yy} = \sigma$  and  $\sigma_{xx} = \sigma_{xy} = 0$ . In general, all two-dimensional stress fields may be represented by a pair of analytic functions (Muskhelishvili, 1975)  $\phi(z)$  and  $\psi(z)$ , where

$$\sigma_{xx} + \sigma_{yy} = 2(\phi'(z) + \bar{\phi}'(\bar{z})) \quad (2)$$

and

$$\sigma_{yy} - \sigma_{xx} + i2\sigma_{xy} = 2(\bar{z}\phi''(z) + \psi'(z)), \quad (3a)$$

$$\sigma_{\theta\theta} - \sigma_{rr} + i2\sigma_{r\theta} = 2(\bar{z}\phi''(z) + \psi'(z))e^{2i\theta}. \quad (3b)$$

We loosely refer to these two analytic functions as “complex potentials”, and it can be straightforwardly shown that they take the form

$$\phi_0(z) = \frac{\sigma}{4}z, \quad \psi_0(z) = \frac{\sigma}{2}z \quad (4)$$

for the uniaxial field described above. These complex potentials can be expressed in terms of the mapped variable,  $\zeta$ , using Eq. (1):

$$\phi_0(\zeta) = \frac{\sigma}{4}R \left( \zeta + \frac{m}{\zeta} \right), \quad \psi_0(\zeta) = \frac{\sigma}{2}R \left( \zeta + \frac{m}{\zeta} \right). \quad (5)$$

To find the complex potentials for a uniaxially loaded plane with an elliptical hole, a second set of complex potentials must be superposed with the complex potentials for the plane under uniaxial tension such that the boundary of the elliptical hole becomes traction free. The complex potentials which satisfy this condition are often referred to as the image terms,  $\phi_{im}$  and  $\psi_{im}$ .

To find these image terms, an expression for the resultant force vector must be introduced. The resultant force vector acting on any continuous arc from  $A$  to  $B$  can be expressed in terms of the complex potentials  $\phi$  and  $\psi$  (Muskhelishvili, 1975):

$$F_x + iF_y = -i[\phi(z) + z\bar{\phi}'(\bar{z}) + \bar{\psi}(\bar{z})]_A^B, \quad (6)$$

Given that the boundary of the ellipse must be traction free, Eq. (6) must vanish for all values of  $z$  on the elliptical boundary,

$$(\phi_0(z) + \phi_{\text{im}}(z)) + z(\bar{\phi}'_0(\bar{z}) + \bar{\phi}'_{\text{im}}(\bar{z})) + (\bar{\psi}_0(\bar{z}) + \bar{\psi}_{\text{im}}(\bar{z})) = 0. \quad (7)$$

In the  $\xi$ -plane, the transformation of this equation holds for all values of  $\zeta$  on the unit circle and is given by

$$(\phi_0(\zeta) + \phi_{\text{im}}(\zeta)) + \frac{1}{\zeta} \frac{(\zeta^2 + m)}{(1 - m\zeta^2)} (\bar{\phi}'_0(\bar{\zeta}) + \bar{\phi}'_{\text{im}}(\bar{\zeta})) + (\bar{\psi}_0(\bar{\zeta}) + \bar{\psi}_{\text{im}}(\bar{\zeta})) = 0. \quad (8)$$

Since the complex potentials must be analytic outside the circular boundary, the image terms can be found using the following Cauchy integrals described by Vitek (1975) where the contour  $\kappa$  lies on the unit circle of the  $\zeta$ -plane,

$$\phi_{\text{im}}(\zeta) = \frac{1}{2\pi i} \int_{\kappa} \left[ \phi_0(\eta) + \frac{1}{\eta} \frac{(\eta^2 + m)}{(1 - m\eta^2)} \bar{\phi}'_0(\bar{\eta}) + \bar{\psi}_0(\bar{\eta}) \right] \frac{1}{\eta - \zeta} d\eta, \quad (9)$$

$$\begin{aligned} \psi_{\text{im}}(\zeta) = & \frac{1}{2\pi i} \int_{\kappa} \left[ \bar{\phi}_0(\bar{\eta}) + \eta \frac{(1 + m\eta^2)}{(\eta^2 - m)} \phi'_0(\eta) + \psi_0(\eta) \right] \frac{1}{\eta - \zeta} d\eta \\ & - \zeta \frac{(1 + m\zeta^2)}{(\zeta^2 - m)} \phi'_{\text{im}}(\zeta). \end{aligned} \quad (10)$$

Substituting the complex potentials  $\phi_0$  and  $\psi_0$  from Eq. (5) and simplifying gives

$$\phi_{\text{im}}(\zeta) = \frac{1}{2\pi i} \int_{\kappa} \frac{\sigma R}{2} \left[ \frac{(1 + m)(1 + \eta^2)}{\eta(\eta - \zeta)} \right] d\eta, \quad (11)$$

$$\psi_{\text{im}}(\zeta) = \frac{1}{2\pi i} \int_{\kappa} \frac{\sigma R}{2} \left[ \frac{(1 + m)(1 + \eta^2)}{\eta(\eta - \zeta)} \right] d\eta - \zeta \frac{(1 + m\zeta^2)}{(\zeta^2 - m)} \phi'_{\text{im}}(\zeta). \quad (12)$$

Using the method of residues and evaluating for the pole at  $\zeta = 0$  gives the image terms, resulting in the complete set of complex potentials for a plane with an elliptical hole under uniaxial tension

$$\phi(\zeta) = \phi_0(\zeta) + \phi_{\text{im}}(\zeta) = \frac{\sigma R}{4} \left( \zeta - (2 + m) \frac{1}{\zeta} \right), \quad (13)$$

$$\psi(\zeta) = \psi_0(\zeta) + \psi_{\text{im}}(\zeta) = \frac{\sigma R}{2} \left( \zeta - \frac{1}{\zeta} - \frac{(1 + m)(1 + m\zeta^2)}{\zeta(\zeta^2 - m)} \right). \quad (14)$$

The chain rule is used to find derivatives with respect to  $z$ :

$$\phi'(z) = \frac{d\phi(\zeta)}{d\zeta} \frac{d\zeta}{dz}, \quad \phi''(z) = \frac{d\phi'(z)}{d\zeta} \frac{d\zeta}{dz}, \quad \psi'(z) = \frac{d\psi(\zeta)}{d\zeta} \frac{d\zeta}{dz}. \quad (15)$$

These values are then used as in Eqs. (2) and (3) to find the overall stress field.

The same method is used to find the dislocation self-stress in the vicinity of an elliptical hole. First, the complex potentials for a dislocation located at position  $z_d$  in

a plane with *no* hole must be considered. These are given by Vitek (1975) as

$$\phi_0^d(z) = \gamma \ln(z - z_d), \tag{16}$$

$$\psi_0^d(z) = \bar{\gamma} \ln(z - z_d) - \gamma \frac{\bar{z}_d}{(z - z_d)}, \tag{17}$$

where

$$\gamma = \frac{\mu b e^{i\alpha}}{4\pi i(1 - \nu)}, \tag{18}$$

and  $\mu$  is the shear modulus,  $b$  is the magnitude of the Burgers vector, and  $\alpha$  is the orientation of the Burgers vector with respect to the horizontal, or in our case, the angle of inclination of the slip plane. Once again, these complex potentials must be transformed to the  $\zeta$ -plane using the transformation given by Eq. (1)

$$\phi_0^d(\zeta) = \gamma \ln \left[ R \left( \zeta + \frac{m}{\zeta} \right) - R \left( \zeta_d + \frac{m}{\zeta_d} \right) \right], \tag{19}$$

$$\psi_0^d(\zeta) = \bar{\gamma} \ln \left[ R \left( \zeta + \frac{m}{\zeta} \right) - R \left( \zeta_d + \frac{m}{\zeta_d} \right) \right] - \gamma \frac{R(\bar{\zeta}_d + (m/\bar{\zeta}_d))}{[R(\zeta + (m/\zeta)) - R(\zeta_d + (m/\zeta_d))]} \tag{20}$$

The mapped dislocation position  $\zeta_d$  is related to  $z_d$  through Eq. (1). As was carried out for the uniaxially loaded problem, these complex potentials must be superposed with a second set of complex potentials, the image terms, in order to obtain the complex potentials for a dislocation in the vicinity of an elliptical hole. This superposition results in a traction free boundary at the elliptical hole, for which the following expression must be true for all  $\zeta$  on the unit circle:

$$(\phi_0^d(\zeta) + \phi_{im}^d(\zeta)) + \frac{1}{\zeta} \frac{(\zeta^2 + m)}{(1 - m\zeta^2)} (\bar{\phi}_0^{d'}(\bar{\zeta}) + \bar{\phi}_{im}^{d'}(\bar{\zeta})) + (\bar{\psi}_0^d(\bar{\zeta}) + \bar{\psi}_{im}^d(\bar{\zeta})) = 0. \tag{21}$$

The image terms are extracted using the Cauchy integrals of Eqs. (9) and (10). Employing the method of residues and adding the original complex potentials (Eqs. (16) and (17)) to the image terms gives the complex potentials for a dislocation in proximity to an ellipse

$$\begin{aligned} \phi^d(z) = & \gamma \ln(z - z_d) + 2\gamma \ln \zeta - \gamma \ln \left( \zeta - \frac{m}{\zeta_d} \right) - \gamma \ln \left( \zeta - \frac{1}{\bar{\zeta}_d} \right) \\ & + \bar{\gamma} \frac{[\zeta_d(1 + m\bar{\zeta}_d^2) - \bar{\zeta}_d(\zeta_d^2 + m)]}{\zeta_d \bar{\zeta}_d (\bar{\zeta}_d^2 - m)(\zeta - (1/\bar{\zeta}_d))}. \end{aligned} \tag{22}$$

$$\begin{aligned} \psi^d(z) = & \bar{\gamma} \ln(z - z_d) - \gamma \frac{\bar{z}_d}{(z - z_d)} + 2\bar{\gamma} \ln \zeta - \bar{\gamma} \ln \left( \zeta - \frac{m}{\zeta_d} \right) - \bar{\gamma} \ln \left( \zeta - \frac{1}{\bar{\zeta}_d} \right) \\ & + \gamma \frac{[\bar{\zeta}_d(\zeta_d^2 + m^3) - m\zeta_d(\bar{\zeta}_d^2 + m)]}{\zeta_d \bar{\zeta}_d (\zeta_d^2 - m)(\zeta - (m/\zeta_d))} - \zeta \frac{1 + m\zeta^2}{\zeta^2 - m} \phi_{im}^{d'}(\zeta). \end{aligned} \tag{23}$$

Eq. (15) is used to obtain derivatives with respect to  $z$ .

It is important to recognize that multiple solutions for the edge dislocation self stress exist, as discussed by Zhang and Li (1991). These solutions account for the distinct situations of dislocation origination at the crack tip or at infinity. The importance of this distinction is that only one of these solutions is stress free when the dislocation is removed to the elliptical boundary. The current solution is applicable for the dislocation originating at infinity, which can be verified by setting  $z_d = a$  in the equations for the complex potentials to obtain a nonzero result. In order to obtain the desired solution (dislocation origination at the ellipse), it is necessary to *subtract* the solution for a dislocation located on the elliptical boundary ( $z_d = a$  and  $\zeta = 1$ ). This superposition of solutions provides a stress free solution in the limiting case when the dislocation is at the boundary of the ellipse.

The applied stress and the dislocation self-stress are used in the governing integral equation,

$$\tau[\delta(r)] = \sigma_{r\theta}(r) - \frac{1}{b} \int_0^\infty \sigma_{r\theta}^{\text{self}}(r, s) \frac{\partial \delta}{\partial s} ds, \quad (24)$$

with  $z = a + re^{i\theta}$  and  $z_d = a + se^{i\theta}$ . The shear stress due to applied loads, assuming a completely elastic response, is represented by  $\sigma_{r\theta}(r)$  and is obtained by combining Eqs. (13), (14), and (15) with (3b). The dislocation self stress is represented by  $\sigma_{r\theta}^{\text{self}}(r, s)$ , and is obtained by combining Eqs. (22), (23), and (15) with (3b). The restoring shear stress due to local slip displacement is represented by  $\tau[\delta(r)]$ . In this paper, the simplest periodic relationship between shear stress and slip displacement along the slip plane of interplanar spacing  $h$  is assumed for  $\tau[\delta(r)]$ . We use the Frenkel (1926) relation

$$\tau[\Delta(r)] = \left( \frac{\mu b}{2\pi h} \right) \sin\left( \frac{2\pi \Delta(r)}{b} \right) = \frac{\pi \gamma_{\text{us}}}{b} \sin\left( \frac{2\pi \Delta(r)}{b} \right) \quad (25)$$

where  $\tau$  is the restoring stress,  $\Delta(r)$  is the relative atomic shear displacement between two atomic planes at any position  $r$  along the slip plane, and  $\gamma_{\text{us}}$  is the unstable stacking energy. The continuum analog to  $\Delta$ , known as  $\delta$ , was introduced by Rice (1992). While  $\Delta$  represents the relative displacement between the centers of two atoms,  $\delta$  is the extrapolation of  $\Delta$  to an imaginary cut halfway between the slipping planes of atoms, and is given by

$$\delta(r) = \Delta(r) - \frac{\tau[\Delta(r)]h}{\mu}. \quad (26)$$

Fig. 2 shows a stylized representation of the  $\tau$  versus  $\Delta$  and  $\tau$  versus  $\delta$  relationships, both of which have a periodicity of one Burgers vector.

In our solution of Eq. (24), we seek a slip distribution  $\delta(r)$  such that for all  $r > 0$ , the shear stress on the slip plane predicted by the linear elastic formulation (the right-hand side of Eq. (24)) must equal the shear stress provided by the atomic-based relation (Eq. (25)). The numerical procedure is described by Beltz and Rice (1992). The slip distribution is solved for increasing values of the applied mode I stress intensity factor (defined as  $\sigma\sqrt{\pi a}$ ) up to the point of instability, beyond which the governing integral equation can no longer be satisfied. The stress intensity immediately prior to instability

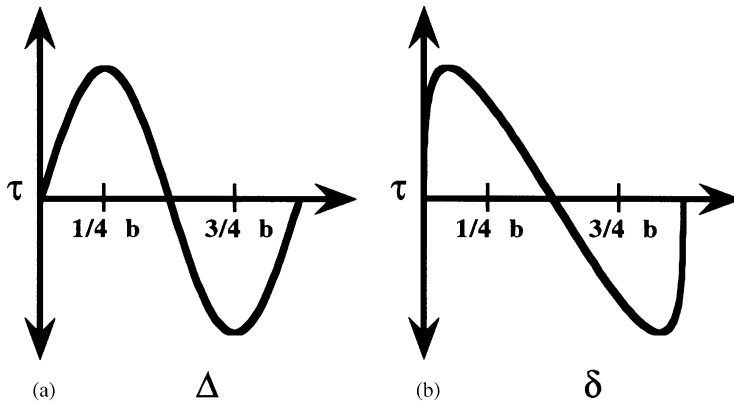


Fig. 2. The shear stress versus slip displacement between two atomic planes ( $\tau$  versus  $\Delta$ ) and the shear stress versus slip displacement at a cut half way between those two atomic planes ( $\tau$  versus  $\delta$ ).

is used to calculate the critical energy release rate for dislocation nucleation, using the Irwin relation for mode I:

$$G = \frac{K^2}{E^*}, \quad (27)$$

where  $E^*$  for plane strain is given by  $E/(1 - \nu^2)$ . Since  $G$  varies monotonically with  $K$ , the mode I stress intensity factor, it is typically used as a measure of the applied load.

Fig. 3 shows the critical energy release rates for various values of crack length and crack tip curvature for a slip plane inclined at  $\theta = 60^\circ$ . For all calculations in this section, we have taken  $h/b = 1.414$  and  $\nu = 0.3$ . The results show that for very short cracks, the threshold for dislocation nucleation is reduced. This effect has been shown to be tied to the  $T$ -stress, that is, a normal component of stress parallel to the crack plane (Beltz and Fischer, 2000), and will not be addressed further in this paper since it is likely not intrinsically connected with crack blunting. It is also clear that increasing the crack tip radius of curvature at very small curvatures decreases the threshold for dislocation nucleation, but at larger curvatures, increases the threshold. This is a reasonable result when one considers a comparison of the stresses ahead of a sharp crack and a very sharp elliptical tip. While the actual peak stress of the sharp crack tip is larger, the stress of the elliptical tip is larger over a greater distance from the crack tip. Recalling that a Peierls-type calculation considers the entire slip plane, it is conceivable that the blunted crack tip, over a limited range of curvatures, will form a dislocation more efficiently than the perfectly sharp crack tip. This would persist until the crack tip becomes so blunt that the stress field throughout the formation zone eventually drops to levels below those of the sharp crack. Note that in the case of the  $60^\circ$  slip plane inclination, the critical energy release rate of dislocation nucleation eventually surpasses the sharp crack threshold when the ellipse has a crack tip curvature of about five Burgers vectors.

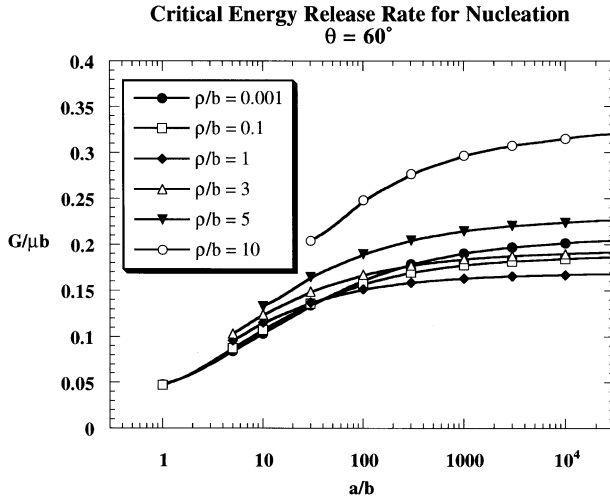


Fig. 3. Critical energy release rates of dislocation nucleation for various crack lengths and crack tip curvatures for mode I loading of an elliptically shaped crack with a slip-plane inclination of  $\theta = 60^\circ$ .

At first glance, it may seem unphysical to provide results for  $\rho$  on the order of one atomic spacing or less. As discussed in Section 2, there are several possible sources of blunting on the atomic scale, such as prior dislocation nucleation. The emission of a single dislocation would impart a step of approximately  $b$ ; hence, we associate this as the characteristic length of blunting, and feel justified in claiming  $\rho \approx b$  in this case. Of course, this is an approximation, in that we use continuum mechanics at the extreme lower length scale at which it is valid. Our motivation for using a few values of  $\rho$  less than  $b$  is primarily mathematical: we needed to verify that our solutions approach the limiting case of a sharp crack in the limit as  $\rho \rightarrow 0$ . Moreover, the framework we propose in Section 5 makes use of a conceptual smooth transition from a sharp crack to a blunt crack.

When we use the results of this section to discuss ductile versus brittle response (Section 5), several additional factors should be kept in mind:

(a) Our determination of the threshold load for dislocation nucleation has not explicitly considered the effects of tensile stress across the slip plane. Argon (1987) has argued that shear softening by tensile forces across the slip plane is a critical element in dislocation nucleation. Several analyses of this effect have appeared, including work by Sun et al. (1993), Beltz and Freund (1994), Xu et al. (1995, 1997), and Beltz and Fischer (1999). The latter studies quantify this effect through the use of a reduced value of  $\gamma_{us}$ , that is, the area under the stress versus displacement curves of Fig. 2.

(b) Several studies of crack tip dislocation nucleation suggest that ledge formation at the crack (which must occur if the nucleated dislocation has an edge component of the Burgers vector) gives rise to an extra resistance to slip, localized just near the crack tip. Atomistic studies by Gumbsch and Beltz (1995) suggest this might partially explain why continuum models for dislocation nucleation tend to underestimate the loads

observed in atomistic models. Xu et al. (1995, 1997) have proposed a modification to Eq. (25) that accounts for this effect, as well as tension-shear coupling. For mode III cracks with the same elliptical geometry as used in this paper, Beltz and Fischer (1999) found a weak to moderate increase in the critical  $G$  for dislocation nucleation when incorporating this ledge effect, and a weak to moderate decrease when incorporating tension-shear coupling — not inconsistent with earlier studies.

(c) Since dislocation nucleation (which is really thought to occur in the form of incipient loops) is a three-dimensional process, susceptible to thermal activation, our (inherently 2D) model neglects these aspects — that is, it is essentially appropriate for the temperature  $T = 0$  response. It is generally thought that an increase in  $T$  eases dislocation nucleation.

(d) Dislocation processes not directly associated with nucleation from a crack tip may actually control mechanical response in many situations. The relative ease or difficulty of dislocation nucleation in a solid with low dislocation mobility (e.g., silicon) may be irrelevant if dislocations cannot be sufficiently swept away from the crack tip region. In the other extreme, solids with a high density of mobile dislocations may never build up enough stress at a crack tip to meet a dislocation nucleation (or fracture) threshold, again rendering dislocation nucleation an irrelevant phenomenon.

#### 4. Atomic decohesion

The most commonly used method to study brittle crack advance is the Griffith (1920) theory, that is, the critical  $G$  for fracture is given by  $2\gamma_s$  ( $\gamma_s$  is the surface energy). Later developments include the cohesive zone model of atomic decohesion (Barenblatt, 1959, 1962), which is very similar to the Peierls treatment of dislocation nucleation in that a relationship between the stress and displacement is assumed to exist along the entire length of the plane ahead of a crack. This relationship is intended to capture the nonlinear aspects of atomic separation. In the cohesive zone model, the stress versus displacement relationship is no longer periodic in nature, and is oftentimes taken as a universal bonding relation described by Smith and Banerjea (1988) and Hong et al. (1994, 1995).

By representing the opening displacement along the crack front as a continuous distribution of infinitesimal dislocations oriented such that their extra half planes point towards the crack front as seen in Fig. 4, a modified version of Eq. (24) can be used as the governing integral equation

$$\sigma[\delta(r)] = \sigma_{yy}(r) - \frac{1}{b} \int_0^\infty \sigma_{yy}^{\text{self}}(r,s) \frac{\partial \delta}{\partial s} ds. \quad (28)$$

This equation reflects the equivalence between an opening profile and an array of dislocations. The analysis presented in this section involves replacing the usual sharp crack with an elliptical crack in order to understand the effect of blunting on continued crack advance.

To physically describe the atomic decohesion of two previously unstressed atoms, an increasing applied tensile stress is required to increase the separation between the

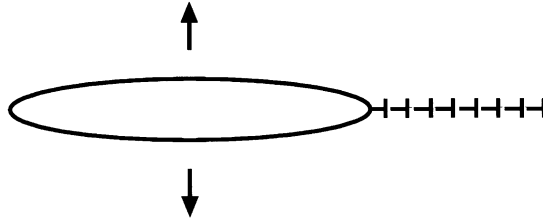


Fig. 4. Infinitesimal dislocations representing the distribution of opening displacement along a crack front with a tensile component of loading.

two atoms until a peak stress is reached, beyond which the attractive forces of the two atoms begin to decay. In our case, the opening stress due to opening displacement is taken as universal bonding relation mentioned earlier,

$$\sigma = \frac{2\gamma_s \Delta}{L^2} e^{-\Delta/L} \quad (29)$$

where  $L$  is the separation of the two atomic centers at the peak stress in the tensile stress versus opening displacement relationship (can be thought of as the characteristic length associated with decohesion). The peak stress is then simply found by substituting  $L$  for  $\Delta$  in Eq. (29) to obtain  $\sigma_p = (2\gamma_s/L)e^{-1}$ . The variable  $\delta$  is the continuum analog to  $\Delta$ ,

$$\delta = \Delta - \frac{L^2 \sigma}{2\gamma_s}. \quad (30)$$

We note that the variables  $\Delta$  and  $\delta$  are used here to denote atomic separation, although we use the same notation to represent *slip* displacement in the previous section.

From this point on, the cohesive zone analysis is nearly analogous to the dislocation nucleation analysis. The differences are that the stresses are tensile rather than shear along a crack plane, and the plane undergoing separation is not inclined (which simplifies the analysis). The same complex potentials derived in Section 3 are applicable to the cohesive zone model. Here, the stress component  $\sigma_{yy}$  is required, which is obtained by combining Eqs. (2) and (3a):

$$\sigma_{yy} = 2\text{Re}\{\phi'(z)\} + \text{Re}\{\bar{z}\phi''(z) + \psi'(z)\}. \quad (31)$$

The solution procedure is identical to that for Eq. (24). Fig. 5 shows the critical energy release rates associated with decohesion for several values of crack tip radius of curvature. We ultimately intend to compare these results with those for dislocation nucleation, hence, all variables have been normalized just as in Section 3 (Fig. 3). This requires the specification of the ratios  $\gamma_{us}/2\gamma_s$  (which we subsequently denote as  $q$ ) and  $L/b$ . For this case,  $q = 0.125$ , which is characteristic of a more ductile material, and  $L/b = 0.25$  (this corresponds to a peak stress  $\sigma_p/E^* \approx 0.15$ ). The results indicate that increasing the crack length increases the threshold for atomic decohesion. More importantly, increasing the crack tip radius of curvature also increases the threshold for atomic decohesion. Unlike dislocation nucleation, there is no initial depression of

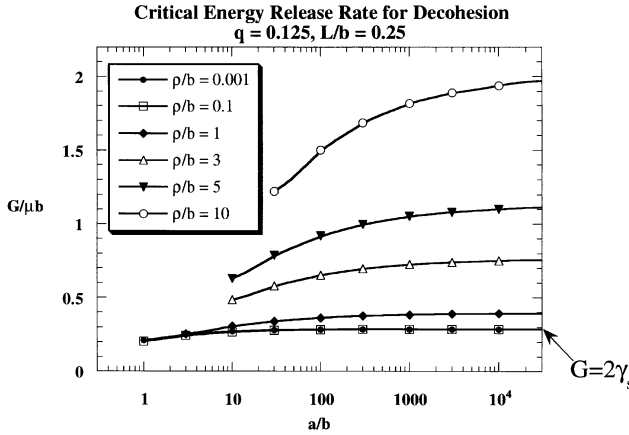


Fig. 5. Critical energy release rates of atomic decohesion for various crack lengths and crack tip radii of curvature for mode I loading of an elliptically shaped crack with  $q = \gamma_{us}/2\gamma_s = 0.125$  and  $L/b = 0.25$ .

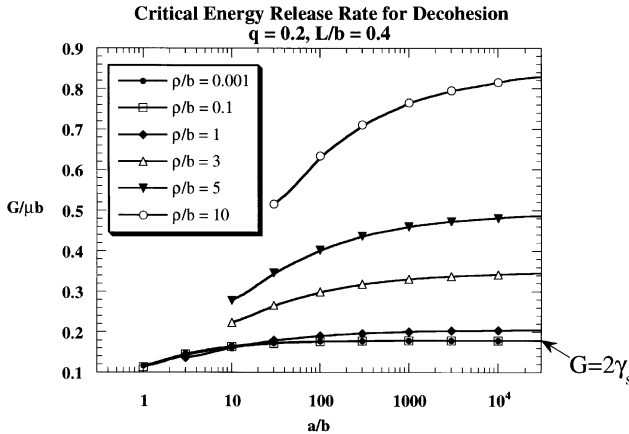


Fig. 6. Critical energy release rates of atomic decohesion for various crack lengths and crack tip radii of curvature for mode I loading of an elliptically shaped crack with  $q = 0.2$  and  $L/b = 0.4$ .

the threshold for slight increases in blunting. In fact, atomic decohesion appears to be more sensitive to the effects of blunting and increases quickly with increases in  $\rho/b$ .

In Fig. 6, the parameter values are changed to  $q = 0.2$  and  $L/b = 0.4$  (corresponds to a peak stress  $\sigma_p/E^* \approx 0.058$ ). The general trends are identical. For very sharp cracks, the Griffith condition is recovered in both cases, i.e., the critical  $G/\mu b$  for fracture is given by  $2\gamma_s/\mu b$  or  $(2q\pi^2 h/b)^{-1}$ . While  $\sigma_p$  has no effect on sharp cracks, it does appear to play a role in the threshold for blunt cracks, an effect which is discussed in further detail by Beltz et al. (1999).

## 5. Ductile versus brittle behavior

The competition between slip processes and decohesive processes is not only competitive, but also an interactive one, in which incipient shear on one slip plane may affect incipient opening on the crack plane or vice versa. The interaction these processes has been studied by Beltz and Schmauder (1994) and we will work with the approximation that each process is isolated. Accepting this limitation, as well as the others discussed at the end of Section 3, we now consider whether conditions for dislocation nucleation will or will not be met prior to cleavage, in the spirit of Rice and Thomson's (1974) model. In this section, the solutions for the dislocation nucleation and atomic decohesion thresholds will be compared for various realistic material parameters. We show that four broad possibilities exist, and that materials should be classified with consideration of the *ongoing* competition between crack propagation and dislocation nucleation as the crack tip curvature evolves. We limit our analyses to a relatively long crack ( $a/b = 10^4$ ) so that some of the short crack effects (as seen in Figs. 3, 5, and 6) may be ignored.

### 5.1. Intrinsically brittle behavior

Intrinsically brittle materials cleave rather than nucleate dislocations from a crack tip when loaded. Griffith's theory has traditionally been used to determine the critical energy release rate of cleavage for these materials. This theory assumes a perfectly sharp crack tip, which is a good assumption for materials that have large dislocation nucleation thresholds. However, other methods are required to calculate the critical load to initiate crack from an initial flaw that is not crack-like. Using the Rice–Thomson model, many materials can be classified as intrinsically brittle. Recall, however, that (1) only sharp cracks are used for this calculation, and (2) only the first dislocation nucleation is considered. Therefore, a material that does not emit dislocations when the crack tip is perfectly sharp, but that may emit dislocations when the crack tip has a radius of curvature of several Burgers vectors, is still classified as intrinsically brittle in the Rice–Thomson model.

Considering the effects of crack tip geometry makes it possible for us to draw a distinction between intrinsically brittle and quasi-brittle fracture. The intrinsically brittle material ought to be defined as one that will cleave prior to dislocation nucleation for *all* values of crack tip radius of curvature. Therefore, the critical energy release rate associated atomic decohesion will be less than the critical energy release rate for dislocation nucleation for all values of crack tip radius of curvature. The types of materials that generally exhibit intrinsically brittle fracture behavior are ceramics below their ductile-to-brittle transition temperature and glasses below their glassy transition temperature. At room temperature, plastic deformation is negligible in these types of materials due to strong ionic or covalent bonding and complex atomic structures. Since glasses have an amorphous atomic structure, the Peierls treatment for dislocation formation is not applicable, but the crystalline structures of some ceramics can be considered. Some of the more common ceramic crystalline configurations are diamond cubics and rock salts. Silicon is a crystalline semiconductor with a di-

Table 1  
Silicon material parameters

$\nu$	$h/b$	$\theta$	$L/b$	$\gamma_{us}$ (J m <sup>-2</sup> )	$\gamma_s$ (J m <sup>-2</sup> )	$q$
0.218	0.354	54.7°	0.308	2.02	1.56	0.647

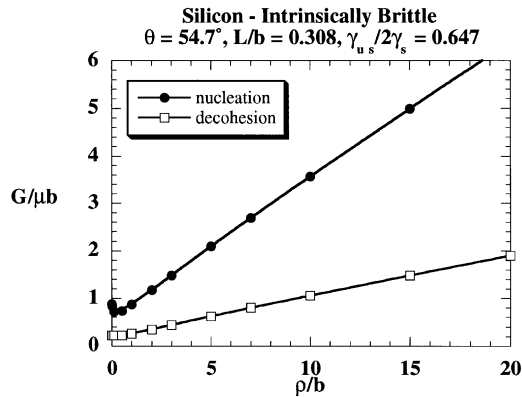


Fig. 7. Comparison of atomic decohesion and dislocation nucleation thresholds in silicon, an intrinsically brittle material.

among cubic structure, and we use it as an example of intrinsically brittle material behavior.

Here, the physical parameters for silicon used to guide our calculation are found in Sun et al. (1993) and Beltz (1992), and are summarized in Table 1. Essentially,  $\gamma_{us}$  and  $\tau_p$  are large compared with  $2\gamma_s$  and  $\sigma_p$ , respectively. Fig. 7 shows the critical energy release rates of dislocation nucleation and atomic decohesion for the described silicon slip system. In this case, the critical energy release rate associated with atomic decohesion is lower than the critical energy release rate for dislocation nucleation for all values of crack tip radius of curvature — thus indicating that silicon is intrinsically brittle. Although we have chosen a specific slip geometry, the basic conclusion holds for other geometries as well.

## 5.2. Quasi-brittle behavior

Like the intrinsically brittle material, the quasi-brittle material generally cleaves rather than emits dislocations from a relatively sharp crack tip that is loaded. However, at some finite radius of curvature of the crack tip, the dominant behavior becomes dislocation nucleation. Since an initially sharp crack cleaves (stays sharp), the only way to contemplate this scenario would be for a blunt crack to evolve from some other mechanism than dislocation nucleation from a sharp crack, e.g., removal of material via a chemical interaction, diffusion, or mechanically. This type of material would be characterized as intrinsically brittle by the Rice–Thomson analysis, but the likelihood

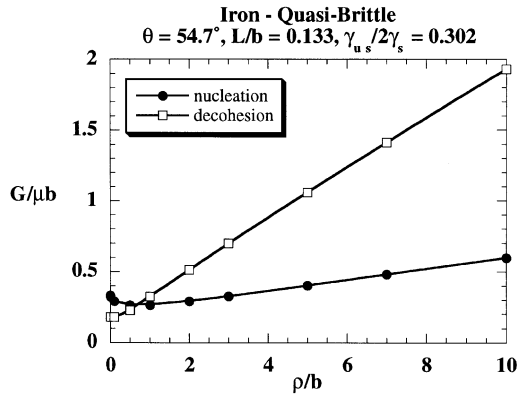


Fig. 8. Ductile versus brittle comparison for iron, indicating quasi-brittle behavior.

Table 2  
Iron material parameters

$\nu$	$h/b$	$\theta$	$L/b$	$\gamma_{us}$ (J m <sup>-2</sup> )	$\gamma_s$ (J m <sup>-2</sup> )	$q$
0.290	0.943	54.7°	0.133	0.860	1.42	0.302

of cleavage would be ultimately lower than for the types of materials previously discussed. The Rice–Thomson theory has no means of determining under what conditions this type of material may nucleate dislocations rather than cleaving, because it only considers sharp cracks.

Using the present analysis, the conditions (or parameters) that would favor this kind of behavior can be suggested. Initially, the critical energy release rate associated with atomic decohesion will be lower than that for dislocation nucleation (see Fig. 8), which suggests that a sharp crack will remain sharp in this type of material. However, if an initial flaw can somehow be introduced (rather than evolving from a sharp crack) that has a radius of curvature that is larger than some crossover value (the intersection of the two energy release curves), the material will nucleate dislocations provided that there are no local perturbations in the crack tip that may initiate stable cleavage. We speculate that certain bcc metals might fall into this definition of “quasi-brittle” material behavior.

Using the physical parameters for  $\alpha$ -Fe, primarily obtained from work done by Shastry and Farkas (1996), the thresholds for dislocation nucleation in the  $(1/2)[11\bar{1}](\bar{2}1\bar{1})$  slip system for a crack running on the  $(01\bar{1})$  plane, in the  $[011]$  direction, are calculated. The material property values used to calculate the critical energy release rate curves in Fig. 8 are summarized in Table 2. The curves suggest that this slip system of iron does exhibit quasi-brittle behavior — but that it may be a very unstable situation. The region over which cleavage is the dominant mechanism is very narrow, and requires that there be essentially no crack blunting to propagate in a brittle fashion. A

Table 3  
Aluminum material parameters

$\nu$	$h/b$	$\theta$	$L/b$	$\gamma_{us}$ (J m <sup>-2</sup> )	$\gamma_s$ (J m <sup>-2</sup> )	$q$
0.345	0.4142	70.5°	0.279	0.0920	0.565	0.0814

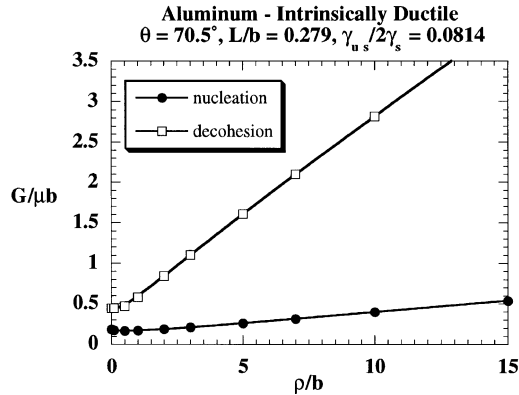


Fig. 9. Comparison of atomic decohesion and dislocation nucleation thresholds in aluminum, an intrinsically ductile material.

crack tip curvature of approximately one Burgers vector makes dislocation nucleation the energetically favorable mechanism. However, as previously discussed, any local perturbation to the crack tip curvature could reinitiate brittle behavior.

### 5.3. Intrinsically ductile behavior

In direct contrast with an intrinsically brittle material, the intrinsically ductile material will always nucleate dislocations regardless of the initial crack geometry. For intrinsically ductile materials, we calculate the thresholds for dislocation nucleation and atomic decohesion and note that the value of the dislocation nucleation threshold is lower than the atomic decohesion threshold for all values of crack tip curvature. Also, the extent to which the crack geometry evolution increases the threshold for dislocation nucleation is determined.

Most room temperature fcc metals, such as aluminum, are good examples of intrinsically ductile materials. Their unstable stacking energies are typically low. Using the material properties suggested by Sun et al. (1993) (shown in Table 3), the critical energy release rates of dislocation nucleation are compared to those of atomic decohesion for aluminum. It is obvious from Fig. 9 that dislocation nucleation is preferred for all values of  $\rho$ , indicating that a crack, somehow formed, would blunt rather than advance. As with the purely brittle behavior (e.g., silicon), this result is very insensitive to the actual geometry used for the calculation.

#### 5.4. *Quasi-ductile behavior*

Using the method of categorizing materials by their fracture behavior, outlined here, a quasi-ductile material would be one that nucleates dislocations at very sharp crack geometries, but reinitiates a sharpening of the crack front, via atomic decohesion, upon reaching a significantly blunt crack tip configuration. Like quasi-brittle materials, there is a crossover between the two threshold curves at a specific crack tip curvature. The Rice–Thomson analysis cannot predict this type of behavior because only the first dislocation nucleation is used to determine the overall material fracture behavior.

We speculate that good candidate systems for this type of fracture behavior include metal–ceramic interfaces. It is to be understood, however, that metal/ceramic interfaces represent the crudest application of our theory in its current form, since the present analysis applies to homogeneous, isotropic solids. The metal, being fairly ductile, would initially favor dislocation nucleation and blunting of the crack tip. However, the bonding of these interfaces are not as strong as those of a monolithic material, and cannot continue to support the loads required to promote further blunting and massive dislocation motion within the metal layer. For example, retaining a nominal value of  $\gamma_s$ , while significantly reducing the peak stress  $\sigma_p$ , has been shown possible by introducing certain impurities onto a MgO/Ag or MgO/Al interface (Hong et al., 1994, 1995). Unfortunately, we have found insufficient material data for any particular material system to provide a complete numerical illustration of this case. Further discussion of this “quasi-brittle” behavior has been given by Beltz et al. (1999).

### 6. Summary and conclusions

Until recently, most models for understanding ductile versus brittle response have been based on an analysis of a sharp crack. This has contributed to a disparity between the results of continuum and atomistic studies. In this paper, considering the effects of crack tip blunting on the competition between dislocation nucleation and atomic decohesion has yielded a model that predicts four distinct types of material fracture behavior. Intrinsically brittle material behavior occurs when the threshold for atomic decohesion is lower than the threshold for dislocation nucleation for all values of crack tip radius of curvature. Intrinsically ductile behavior occurs when the threshold for dislocation nucleation is always lower than the threshold for atomic decohesion. Quasi-brittle materials cleave when their crack tips are fairly sharp but will nucleate dislocations if their crack tip curvature is greater than some threshold value while quasi-ductile materials will nucleate dislocations at sharp crack tips and cleave upon reaching a threshold crack tip curvature.

The fundamental assumptions made in this theoretical framework are that the crack tip evolves into an elliptical profile, dislocation nucleation occurs on only one activated slip plane which intersects the crack tip at some angle of inclination, and atomic decohesion occurs directly along the crack front. The framework also utilizes the Peierls-type description of incipient zones of slip and opening displacement, thereby eliminating notions associated with the core cutoff parameter. While we primarily focused on mode

I edge dislocation nucleation, the analysis can very straightforwardly be expanded to account for all three modes of loading and combined edge and screw components.

At present, this model is limited to predicting the early competition between dislocation nucleation and cleavage for an isotropic material, and lacks the ability to account for larger scale phenomena like the accumulation of far field plasticity or the intersection of grain boundaries in a polycrystalline material. For the case of plasticity, the applied energy release rates should rigorously be defined as those based on the local “*screened*” crack tip field, which can differ from the macroscopic field due to other dislocations or nonlinear effects in the system.

The shielding effect of previously emitted dislocations which would result in the geometric blunting of the crack tip can lower the local stress field around the crack and therefore increase the critical applied loads for dislocation nucleation and cleavage. Although emitted dislocations are assumed to be swept sufficiently far away that these shielding effects in the near tip calculations may be ignored, the importance of external dislocations and plastic dissipation on the ductile versus brittle competition have been shown to play a critical role in the actual applied loads necessary to maintain the local loads described in this paper.

In closing, this study has incorporated the effects of crack tip blunting into an analytical methodology for determining the thresholds of competing atomic-scale failure mechanisms. In so doing, the competition between ductile and brittle fracture mechanisms reveals four possible types of material behavior. The respective roles of the parameters  $\gamma_s$ ,  $\gamma_{us}$ ,  $\tau_p$ , and  $\sigma_p$  in this competition have been clarified.

## Acknowledgements

This research was supported by the National Science Foundation under award numbers CMS-9634647 and INT-9707863. Discussions with D.M. Lipkin and D. Farkas proved very helpful in the completion of this work.

## References

- Argon, A.S., 1987. Brittle to ductile transition in cleavage fracture. *Acta Metall.* 35 (1), 185–196.
- Barenblatt, G.I., 1959. The formation of equilibrium cracks during brittle fracture. General ideas and hypotheses. Axially-symmetric crack. *Appl. Math. Mech.* 23, 622.
- Barenblatt, G.I., 1962. The mathematical theory of equilibrium cracks in brittle fracture. *Adv. Appl. Mech.* 7, 55–129.
- Beltz, G.E., 1992. The mechanics of dislocation nucleation at a crack tip. Ph.D. thesis, Harvard University, Cambridge, MA.
- Beltz, G.E., Fischer, L.L., 1999. Effect of finite crack length and blunting on dislocation nucleation in mode III. *Philos. Mag.* A 79 (6), 1367–1378.
- Beltz, G.E., Fischer, L.L., 2000. Effect of T-stress on edge dislocation formation at a crack tip under mode I loading. In: Chuang, T.-J., Rudnicki, J.W. (Eds.), *Multi-Scale Deformation and Fracture in Materials and Structures*. Kluwer, Dordrecht.
- Beltz, G.E., Freund, L.B., 1994. Analysis of the strained-layer critical thickness concept based on a peierls-nabarro model of a threading dislocation. *Philos. Mag.* A 69 (1), 183–202.
- Beltz, G.E., Lipkin, D.M., Fischer, L.L., 1999. Role of crack blunting in ductile versus brittle response of crystalline materials. *Phys. Rev. Lett.* 82 (22), 4468–4471.

- Beltz, G.E., Rice, J.R., 1992. Dislocation nucleation at metal-ceramic interfaces. *Acta Metall. Mater.* 40, S321–S331.
- Beltz, G.E., Schmauder, S., 1994. A multi-plane model for defect nucleation at cracks In: Kvam, E.P., King, A.H., Mills, M.J., Vitek, V. (Eds.), *Defect-Interface Interactions*, Materials Research Society, Warrendale, PA. Vol. 319, pp. 257–262.
- Dienes, G.J., Paskin, A., 1987. Molecular dynamic simulations of crack propagation. *J. Phys. Chem. Solids* 48 (11), 1015–1033.
- Farkas, D., 1998a. Fracture toughness from atomistic simulations: brittleness induced by emission of sessile dislocations. *Scr. Mater.* 39, 533–536.
- Farkas, D., 1998b. Atomistic simulations of fracture in the B2 phase of the Nb-Ti-Al system. *Mater. Sci. Eng. A* 249, 249–258.
- Farkas, D., 1999. Private communication.
- Frenkel, J., 1926. Zur theorie der elastizitätsgrenze und der festigkeit kristallinischer körper. *Z. Phys.* 37, 572–609.
- Griffith, A.A., 1920. The phenomenon of rupture and flow in solids. *Philos. Trans. Roy. Soc. London A* 221, 163–198.
- Gumbsch, P., 1995. An atomistic study of brittle fracture: toward explicit failure criteria from atomistic modeling. *J. Mater. Res.* 10 (11), 2897–2907.
- Gumbsch, P., Beltz, G.E., 1995. On the continuum versus atomistic descriptions of dislocation nucleation and cleavage in nickel. *Modelling Simul. Mater. Sci. Eng.* 3 (5), 597–613.
- Hong, T., Smith, J.R., Srolovitz, D.J., 1994. Metal/ceramic adhesion: a first principles study of MgO/Al and MgO/Ag. *J. Adhesion Sci. Technol.* 8 (8), 837–851.
- Hong, T., Smith, J.R., Srolovitz, D.J., 1995. Theory of metal-ceramic adhesion. *Acta Metall. Mater.* 43 (7), 2721–2730.
- Muskhelishvili, N.I., 1975. *Some Basic Problems on the Mathematical Theory of Elasticity: Fundamental Equations, Plane Theory of Elasticity, Torsion and Bending*. Noordhoff, Holland.
- Paskin, A., Massoumzadeh, B., Shukla, K., Sieradzki, K., Dienes, G.J., 1985. Effect of atomic crack tip geometry on local stresses. *Acta Metall.* 33 (11), 1987–1996.
- Peierls, R.E., 1940. The size of a dislocation. *Proc. Phys. Soc.* 52, 34–37.
- Rice, J.R., 1992. Dislocation nucleation from a crack tip: an analysis based on the Peierls concept. *J. Mech. Phys. Solids* 40 (2), 239–271.
- Rice, J.R., Beltz, G.E., Sun, Y., 1992. Peierls framework for dislocation nucleation from a crack tip. In: Argon, A.S. (Ed.), *Topics in Fracture and Fatigue*. Springer, New York, pp. 1–58.
- Rice, J.R., Thomson, R., 1974. Ductile versus brittle behavior of crystals. *Philos. Mag.* 29 (1), 73–97.
- Schiötz, J., Canel, L.M., Carlsson, A.E., 1997. Effects of crack tip geometry on dislocation emission and cleavage: a possible path to enhanced ductility. *Phys. Rev. B* 55 (10), 6211–6221.
- Schiötz, J., Carlsson, A.E., Canel, L.M., Thomson, R., 1996. Effect of crack blunting on subsequent crack propagation. in: Blumberg Selinger, R.L., Mecholsky, J.J., Carlsson, A.E., Fuller, Jr. E.R. (Eds.), *Fracture — Instability Dynamics, Scaling, and Ductile/Brittle Behavior*. Vol. 409 Materials Research Society, Warrendale, PA, pp. 95–100.
- Shastry, V., Farkas, D., 1996. Molecular statics simulation of fracture in  $\alpha$ -iron. *Modelling Simul. Mater. Sci. Eng.* 4 (5), 473–492.
- Smith, J.R., Banerjee, A., 1988. Equivalent-crystal theory of oscillatory surface relaxation. *Phys. Rev. B* 37 (17), 10,411–10,414.
- Sun, Y., Beltz, G.E., Rice, J.R., 1993. Estimates from atomic models of tension-shear coupling in dislocation nucleation from a crack tip. *Mater. Sci. Eng. A* 170, 67–85.
- Vitek, V., 1975. Yielding from a crack with finite root-radius loaded in uniform tension. *J. Mech. Phys. Solids* 24, 67–76.
- Xu, G., Argon, A.S., Ortiz, M., 1995. Nucleation of dislocations from crack tips under mixed modes of loading: implications for brittle against ductile behaviour of crystals. *Philos. Mag. A* 72 (2), 415–451.
- Xu, G., Argon, A.S., Ortiz, M., 1997. Critical configurations for dislocation nucleation from crack tips. *Philos. Mag. A* 75 (2), 341–367.
- Zhang, T.-Y., Li, J.C.M., 1991. Image forces and shielding effects of an edge dislocation near a finite length crack. *Acta Metall. Mater.* 39 (11), 2739–2744.